13. M. M. Smith, L. Shi, M. Navre, *J. Biol. Chem.* **270**, 6440 (1995).
14. M. M. Poo, *Nature Rev. Neurosci.* **2**, 24 (2001).
15. M. Donovan *et al.*, *Development* **127**, 4531 (2000).
16. Recombinant adenovirus encoding rat BDNF (*27*) was used to infect 293 cells or a temperature-sensitive SV40 T antigen transformed murine cardiac microvascular endothelial cell line at a multiplicity of infection of 100 or 200, respectively. Forty-eight-hours after infection, BDNF in the media was harvested and incubated with plasmin (3 μg/ml; American Diagnostics, Greenwich, CT) with or without (+/−) aproptinin (3 μl/ml; Sigma, St. Louis, MO), MMP-2, -3, -7 (10 μl/ml; Calbiochem, San Diego, CA) or harvested and incubated with MMP-9 (10 μl/ml; Oncogene, Cambridge, MA) with or without (+/−) MMP inhibitor (5 μl/ml, Calbiochem) for 1 hour at 37°C. Purified proNGF (0.8 μg/ml) (*17*) was used for proteolytic digestion in parallel samples. Cleavage products were detected by Western blot analysis using antibody specific for mature BDNF or mature NGF.
17. The cDNA encoding mouse NGF was amplified by reverse transcriptase–polymerase chain reaction (RT-PCR) and was bidirectionally sequenced. To improve translation initiation, 11 bases from mouse 5′ untranslated region (UTR) of mouse NT-3 including the Kozak consensus were exchanged for the mouse NGF sequence [GenBank M35075, base pairs (bp) 84 to 95] immediately 5′ of the initiating methionine. Using PCR-based mutagenesis, six histidine (His) residues were added at the COOH-terminus, and residues RR (bp 1008 to 1013) near the COOH-terminus were mutated to AA to prevent cleavage of the His-tag. To generate proNGF with impaired furin-cleavage, residues RR (bp 531 to 536) were mutated to AA using PCR. After bidirectional sequencing, constructs were subcloned into the expression vector pCDNA and stably transfected 293 cells were isolated after selection in G418 containing medium. Cells were incubated in serum-depleted media for 18 hours, and the media was collected and depleted of cells by centrifugation. His-tagged mature or furin-resistant proNGF was purified using Ni-bead chromatography (Xpress System Protein Purification; Invitrogen, Carlsbad, CA) per manufacturer's methods with the use of 350 mM imidazole for elution. Medium from 293 cells stably transfected with vector alone was harvested in parallel.
18. Mouse NGF (Harlan, Indianapolis, IN) was radioiodinated using lactoperoxidase and hydrogen peroxide as described (*28*) to an average specific activity of 3000 disintegrations per minute (dpm)/fmol and was used within 2 weeks. Competition analysis of equilibrium binding was performed using a whole-cell assay. A875 melanoma cells expressing $p75^{NTR}$ but not Trk receptors or 293 cells stably transfected with pCDNA-rat TrkA (*17*) were resuspended at 0.75×10^6 cells/ml final concentration. Cells were incubated with 1 nM radioiodinated NGF in the presence or absence of unlabeled mature NGF or unlabeled proNGF from 0.005 to 7 nM concentration and binding proceeded for 1 hour at 0.4°C. Cell-bound NGF was separated from free NGF by centrifuging through calf serum. Each condition was assessed in quadruplicate. Nonspecific binding measured in parallel incubation with 500-fold excess mature NGF was less than 10% of total binding. Results corrected for this nonspecific binding were expressed as the mean ± standard deviation. The PRISM program was used to generate the IC_{50} with the use of linear regression.
19. B. L. Hempstead *et al.*, *Nature* **350**, 678 (1991).
20. A. Schropel, D. von Schack, G. Dechant, Y. A. Barde, *Mol. Cell. Neurosci.* **6**, 544 (1995).
21. S. Wang *et al.*, *Am. J. Pathol.* **157**, 1247 (2000).
22. 293 cells expressing TrkA were serum-starved for 18 hours and then neurotrophins were added for 10 min before cell harvest. TrkA was immunoprecipitated with pan-Trk antibody (*19*), and Western blots probed with antibody to phosphotyrosine. TrkA-expressing PC12 cells (*29*) were used for neuritogenesis assays, and freshly isolated SCG from P0 rat pups were used on collagen substrate.
23. S. X. Bamji *et al. J. Cell Biol.* **140**, 911 (1998).
24. J. M. Frade, A. Rodriguez-Tebar, Y.-A. Barde, *Nature* **383**, 166 (1996).
25. P. Cassacia-Bonnefils, B. D. Carter, R. T. Dobrowski, M. V. Chao, *Nature* **383**, 716 (1996).
26. M. J. Donovan *et al.*, *Am. J. Pathol.* **147**, 309 (1995)
27. E. Benraiss *et al.*, *J. Neurosci.* **21**, 6718 (2001).
28. D. Mahadeo *et al.*, *J. Biol. Chem.* **269**, 6884 (1994).
29. B. L. Hempstead *et al.*, *Neuron* **9**, 883 (1992).
30. Supported by NIH grant NS30687, the Burroughs Wellcome Fund and the American Heart Association (to B.L.H.), and NIH grant T32 EY07138. We thank M. Chao, J. Salzer, D. Falcone, I. Feit, K. Hajjar, and S. Rafii for comments; C. Cummins and M. Kobi for technical assistance; and C. Wieland for manuscript preparation. Adenoviral vectors were kindly provided by S. Goldman, and murine endothelial cells were provided by B. Weksler and D. Poulan.

3 August 2001; accepted 25 October 2001

Lobster Sniffing: Antennule Design and Hydrodynamic Filtering of Information in an Odor Plume

M. A. R. Koehl,[1]* Jeffrey R. Koseff,[2] John P. Crimaldi,[2]† Michael G. McCay,[1] Tim Cooper,[1] Megan B. Wiley,[2] Paul A. Moore[3]

The first step in processing olfactory information, before neural filtering, is the physical capture of odor molecules from the surrounding fluid. Many animals capture odors from turbulent water currents or wind using antennae that bear chemosensory hairs. We used planar laser–induced fluorescence to reveal how lobster olfactory antennules hydrodynamically alter the spatiotemporal patterns of concentration in turbulent odor plumes. As antennules flick, water penetrates their chemosensory hair array during the fast downstroke, carrying fine-scale patterns of concentration into the receptor area. This spatial pattern, blurred by flow along the antennule during the downstroke, is retained during the slower return stroke and is not shed until the next flick.

Many animals use chemical cues in the water or air around them to detect mates, competitors, food, predators, and suitable habitats (*1–3*). Large-scale turbulent flow in the environment carries odorants from a source to an animal's olfactory organ (such as an antenna or nose), while small-scale laminar flow near the organ's surface and molecular diffusion transport odorants to the receptors (*2*, *4*). Turbulent fluid motion on a scale of meters to millimeters (*5*) determines the patchy intermittent structure of odor plumes in the environment (*6*); hence, chemical signals monitored at a point downstream from an odor source fluctuate in terrestrial (*7*, *8*) and aquatic (*9*, *10*) habitats and in laboratory flumes (*11–12*). Recent attention has focused on the relation between the neural output of antennae and of the brain antennal lobe of moths in odor plumes (*13*) and on the neural processing of odorant pulses (*14*). We used lateral antennules of spiny lobsters, *Panulirus argus*, to analyze the critical first step in determining the spatial and temporal patterns of odor pulses arriving at receptors: the physical interaction of the olfactory organ with an odor plume. *P. argus* lateral antennules (Fig. 1A) bear rows of aesthetascs (hairs containing hundreds of chemoreceptor cells) flanked by larger guard hairs (*15*) and thus provide a system for investigating the design of hair-bearing olfactory antennae (*16*, *17*).

Fluid flow around a hair in an array depends on the relative importance of inertial and viscous forces, as represented by the Reynolds number (Re) (*18*). Because the fluid in contact with the surface of a moving object does not slip relative to the object, a velocity gradient develops in the flow around the object. The smaller or slower the object (that is, the lower its Re), the thicker this boundary layer of sheared fluid is relative to the size of the object. If the boundary layers around the hairs in an array are thick relative to the gaps between hairs, then little fluid leaks through the array. Hair arrays undergo a transition between nonleaky paddlelike behavior and leaky sievelike behavior as Re is increased (*19–21*). Although flow velocity has only a small effect on the rate of molecule

[1]Department of Integrative Biology, University of California, Berkeley, CA 94720–3140, USA. [2]Environmental Fluid Mechanics Laboratory, Department of Civil and Environmental Engineering, Stanford University, Stanford, CA 94305–4020, USA. [3]Department of Biological Sciences and the J. P. Scott Center for Neuroscience, Mind, and Behavior, Bowling Green State University, Bowling Green, OH 43403, USA.

*To whom correspondence should be addressed. E-mail: cnidaria@socrates.berkeley.edu
†Present address: Department of Civil, Environmental, and Architectural Engineering, University of Colorado, Boulder, CO 80309–0428, USA.

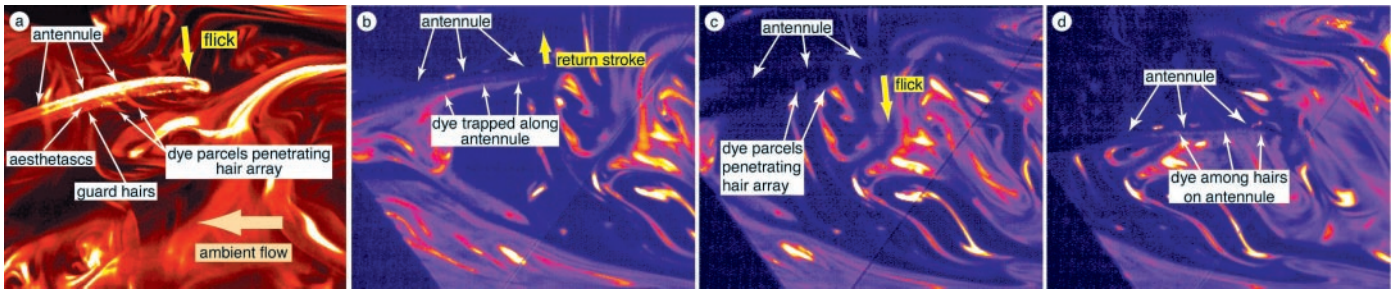

Fig. 1. Video frames of a lobster antennule flicking in a turbulent plume of fluorescent dye illuminated by a vertical sheet of laser light parallel to the flow direction in a flume. Image height, 31.4 mm. The aesthetasc-bearing lateral filament of the antennule is visible in (**A**) but not in (**B** through **D**), in which an optical filter eliminates wavelengths other than the light fluoresced by the dye. The lighter the dye in (A), the higher the dye concentration. Concentration is coded by color in (B) through (D) (see scale in Fig. 2). The plume 1 m downstream from the source is composed of fine parcels of high dye concentration interspersed between layers of clean water. Recognizable features in the plume are carried downstream (that is, they move left) in sequence (B) through (D), which shows the antennule during a return stroke (B) and the next flick downstroke [(C) and (D)]. During the rapid flick [(A)and (C)], water carrying fine strips of dye penetrates into the array of hairs on the antennule. Because the ambient current transports dye along the antennule as it flicks, dye becomes spread along the antennule by the end of the downstroke (D). During the slower return stroke (B) and stationary pause, dye captured during the flick is trapped between the hairs, whereas dye in the ambient current does not penetrate into the array. Trapped water and dye are shed during the next rapid flick (C).

interception by an isolated hair (*4*), our work with arrays of hairs showed that changes in velocity can have a profound impact on odorant encounter rates in the Re range in which the leakiness of the array is sensitive to speed (*2, 22, 23*).

Various crustaceans flick their olfactory antennules in the critical Re range for their particular aesthetasc spacing in which leakiness changes with velocity (*17*, *24*, *25*). High-speed kinematic analysis (*25*) and dynamically scaled physical modeling (*17*) of *P. argus* antennule flicking revealed that water flows through the aesthetasc array during the rapid flick downstroke but not during the slower return stroke. Flicking has been described as "sniffing": a mechanism of enhancing odor penetration into the receptor area, as measured when isolated antennule preparations are hit with pulses of rapid flow (*26–28*). Although many modelers of odor tracking focus on the average properties of a turbulent plume, treating it as a diffusing concentration gradient (*29*), other investigators suggest that the fine-scale spatial patterns of concentration in a plume might provide information animals can use to locate the odor source (*3*, *8*, *30*). Whether animals have access to that information depends on how their olfactory organs disrupt plume structure. We studied how the hydrodynamics of antennule flicking in turbulent plumes physically alters the spatiotemporal patterns of concentration arriving at the aesethetascs.

We programmed a mechanical lobster to flick real *P. argus* antennules in a flume (*31*) in water flow with small-scale turbulence similar to that found in natural lobster habitats (*25*, *32*). Fluorescent dye slowly released from the substratum 1 m upstream from the antennule mimicked odor leaching from a benthic source (*33*). High-speed videos of antennules flicking through a laser-illuminated plane in the dye plume (*34*) showed that the plume was composed of intermittent fine (~1 mm thick) parcels of dye that only penetrated into the aesthetasc array during the flick downstroke (Fig. 1, A and C). By measuring in each video frame the dye concentration along a transect through the aesthetasc array parallel to the length of an antennule, a spatiotemporal map of the concentrations encountered by the aesthetascs along the antennule was constructed (Fig. 2). Such maps showed that the spatial pattern of concentration along an antennule changed during the leaky flick but not during the slow return stroke and stationary pause when the aesthetasc array was much less leaky. Thus, the antennule took a water sample during the flick downstoke and then retained it in the hair array (Fig. 1B) until the next flick (Fig. 1C). In addition, the maps revealed that high-frequency fluctuations in concentration were encountered in the hair array during the downstroke, whereas concentration remained relatively steady during the return and pause (Fig. 2 and Table 1).

To test whether the temporal pattern in concentration variation encountered by the

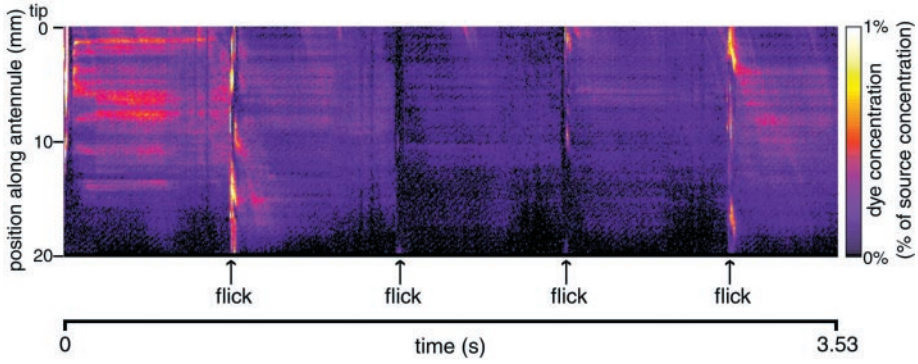

Fig. 2. Spatiotemporal map of dye concentration encountered by the aesethetasc-bearing portion of an antennule. The position along the antennule is plotted on the vertical axis, and time is plotted on the horizontal axis; concentration at each position at each time is indicated by color (yellow is 1% of concentration at the plume source; purple is 0%). A horizontal streak of color indicates that concentration at a position was not changing with time. When a rapid flick downstroke occurred (arrows), the spatial pattern of concentration along the antennule changed, but the new pattern was retained during the slower return stroke and the stationary pause.

Table 1. Mean temporal variance of concentration (% of source) measured at the midpoint of the aesthetasc-bearing section of an antennule for a duration of 44 ms midway during a flick, return, or pause (n = 83 flicks) (*35*).

	Flick ($\%^2 \times 10^{-5}$)	Return ($\%^2 \times 10^{-5}$)	Pause ($\%^2 \times 10^{-5}$)
Real antennule	250	4	4
Virtual antennule	350	96	600

Table 2. Mean spatial variance of concentration (% of source) measured at 210 evenly spaced points along the aesthetasc-bearing section of the antennule at the instant midway during a flick, return, or pause (n = 83 flicks) (*37*).

	Flick ($\%^2 \times 10^{-5}$)	Return ($\%^2 \times 10^{-5}$)	Pause ($\%^2 \times 10^{-5}$)
Real antennule	390	9	32
Virtual antennule	540	370	770

aesthetascs was due to changes in leakiness of the hair array, we compared the temporal variance of concentration at the midpoint of an antennule with that encountered by the midpoint of a virtual antennule that had no physical structure but that swept through the same portion of the plume at the same velocities as the antennule (*34*). Unlike the real antennule, the virtual antennule experienced high temporal variance in concentration during the return and pause as well as during the flick (Table 1). The temporal variance of the real and virtual antennules was similar during the leaky flick (*35*), indicating that the fine details of the plume structure did enter the hair array. In contrast, the temporal variance of the real antennule was much lower than that of the virtual during the nonleaky return and pause (*35*), indicating that the fluctuations in plume structure that occurred during those antennule behaviors were not sampled.

By the end of a flick, the hair-bearing lateral filaments of *P. argus* antennules had blurred the fine-scale structure of the odor plume. This blurring was due to shearing of the water in the aesthetasc array rather than to molecular diffusion (*36*). Even leaky arrays of hairs retain and shear some water near hair surfaces (*2*, *19–24*). Because some dye was retained around the aesthetascs where parcels of dye flowed through the array, and because the ambient current transported those parcels of dye along the length of the antennule as it flicked (Fig. 1, B through D), dye from each parcel was spread along the antennule during the course of the downstroke. Therefore, by the end of the flick, the fine-scale spatial patterns of concentration in the plume had been smeared out in the sample within the aesthetasc array (Fig. 1D). The instantaneous spatial variance in concentration along the length of the antennule at mid-flick was much higher than at mid-return or mid-pause, whereas the spatial variance for the virtual antennule was always high (Table 2) (*37*).

Whether animals can use the fine-scale patterns of concentration in a turbulent plume to locate an odor source (*3*, *7*, *30*) depends not only on neural filtering of that information but also on the fluid dynamics of their olfactory organs. The physical interaction of an olfactory antennule with the surrounding fluid is the first step in filtering the spatial and temporal patterns of concentration in the environment. Because *P. argus* flick their antennules in the Re range in which the leakiness of their aesthetasc array is sensitive to velocity, not only do they sniff (*17*, *25–28*), but they also take samples of plume structure that are discrete in space and time. Fine-scale high-frequency structures of a plume enter the receptor area only during the rapid downstroke but become blurred by the end of the downstroke. The blurred sample is then retained between the aesthetascs until the next flick. The duration of the downstroke is ~100 ms (*25*); although chemoreceptor cells in the anntenules of another species of lobster can respond to very brief (50-ms) pulses of odor, they must be exposed to a pulse for at least 200 ms in order to measure odorant concentration (*38*). Thus, although it is now clear how the hydrodynamics of an antennule filters the spatiotemporal map of concentration arriving at the receptors, which aspects of that information the lobsters use are still unknown.

References and Notes

1. R. T. Cardé, in *Chemical Ecology of Insects*, W. J Bell, R. T. Cardé, Eds. (Elsevier, Amsterdam, 1984), pp. 109–134.
2. M. A. R. Koehl, *Mar. Freshwater Behav. Physiol.* **27**, 127 (1996).
3. M. J. Weissburg, *Biol. Bull.* **198**, 188 (2000).
4. J. D. Murray, *Lectures on Nonlinear-Differential-Equation Models in Biology* (Oxford Univ. Press, Oxford, 1976), pp. 83–127.
5. J. P. Crimaldi, J. R. Koseff, *Exp. Fluids* **31**, 90 (2001).
6. J. Westerberg, in *Proceedings of the 10th International Symposium on Olfaction and Taste*, K. Døving, Ed. (Graphic Communicatons Systems, Oslo, Norway, 1991), pp. 45–65.
7. J. Murlis, in *Mechanisms of Insect Olfaction*, T. L. Payne, Ed. (Clarendon, Oxford, 1986), pp. 27–38.
8. J. Murlis, J. S. Elkinton, R. T. Cardé, *Annu. Rev. Entomol.* **37**, 505 (1992).
9. J. Atema, P. A. Moore, L. P. Madin, G. A. Gerhardt, *Mar. Ecol. Prog. Ser.* **74**, 303 (1991).
10. R. K. Zimmer-Faust, M. Finelli, N. D. Pentcheff, D. S. Wethey, *Biol. Bull.* **188**, 111 (1995).
11. P. A. Moore, J. Atema, *Biol. Bull.* **181**, 408 (1991).
12. P. A. Moore, J. Weissburg, J. M. Parrish, R. K. Zimmer-Faust, G. A. Gerhardt, *J. Chem. Ecol.* **20**, 255 (1994).
13. N. J. Vickers, T. A. Christensen, T. C. Baker, J. G. Hildebrand, *Nature* **410**, 466 (2001).
14. R. W. Freidrich, G. Laurent, *Science* **291**, 889 (2001).
15. U. Grunert, B. W. Ache, *Cell Tissue Res.* **251**, 95 (1988).
16. R. Y. Zacharuk, in *Comprehensive Insect Physiology, Biochemistry and Pharmacology*, G. A. Kerkut, L. I. Gilbert, Eds. (Pergamon, New York, 1985), pp. 1–69.
17. M. A. R. Koehl, *Inst. Math. Appl. Ser.* **124**, 97 (2001).
18. Reynolds number (Re) = lu/ν, where u is velocity, l is hair diameter, and ν is the kinematic viscosity of the fluid.
19. M. A. R. Koehl, *Soc. Exp. Biol. Symp.* **49**, 157 (1995).
20. A. Y. L. Cheer, M. A. R. Koehl, *J. Theor. Biol.* **129**, 185 (1987).
21. _____, *Inst. Math. Appl. J. Math. Appl. Med. Biol.* **4**, 185 (1987).
22. C. Loudon, M. A. R. Koehl, *J. Exp. Biol.* **203**, 2977 (2000).
23. M. Stacey, K. S. Mead, M. A. R. Koehl, *J. Math. Biol.*, in press.
24. K. S. Mead, M. A. R. Koehl, *J. Exp. Biol.* **203**, 3795 (2001).
25. J. A. Goldman, M. A. R. Koehl, *Chem. Senses* **26**, 385 (2001).
26. B. C. Schmidt, B. A. Ache, *Science* **205**, 204 (1979).
27. R. A. Gleeson, W. E. S. Carr, H. G. Trapido-Rosenthal, *Chem. Senses* **18**, 67 (1993).
28. P. A. Moore, J. Atema, G. A. Gerhardt, *Chem. Senses* **16**, 663 (1991).
29. W. H. Bossert, E. O. Wilson, *J. Theor. Biol.* **5**, 443 (1963).
30. J. Atema, *Biol. Bull.* **191**, 129 (1996).
31. A model lobster was made by filling the molted exoskeleton of a *P. argus* (carapace length, 8.6 cm) with epoxy. The lateral filament of the right antennule of the model was replaced by a 2-cm steel wire affixed to a hinge operated by a control rod moved by a software-controlled servo motor. For each experiment, the aesthetasc-bearing lateral filament was removed from the right antennule of a frozen female *P. argus* (carapace lengths, 8.0 to 9.3 cm), thawed in seawater, and slipped like a sock onto the wire of the model's antennule. The model was placed, facing upstream as it would be if tracking an odor plume, on the floor of the flume 1.0 m downstream from the dye source. The antennule lateral filament (6 cm long) was flicked in the sheet of laser light to mimic *P. argus* aesthetasc orientation and flicking kinematics (*25*): The tip moved 6 mm, with the flick downstroke lasting 0.1 s, the upstroke 0.3 s, and the stationary pause 0.4 s. Digitization of video images showed that the curvature of the flexible distal regions of these antennules as they flicked matched that measured for flicking antennules on living *P. argus* (*25*). Only antennules with undamaged arrays of aesthetascs and guard hairs (determined by microscope inspection before and after an experiment) were used. Immersion in fresh water in the flume did not alter the external morphology of the hair arrays. Some experiments were done with a steel model of a lobster body; flow visualizations showed that neither the real nor the steel lobster bodies affected the flow encountered by the antennules. The bodies of living lobsters do not distort odor plumes before they reach the antennules (*30*).
32. We created a laboratory-scale odor plume within a turbulent boundary layer along the bed of a recirculating free-surface flume as described (*5*, *39*). The free stream velocity for this unidirectional flow was 10 cm/s; a 4-m-high constant-head tank produces constant and repeatable flow conditions in the test section. The boundary layer, which was "tripped" by a 3-mm-diameter rod spanning the flume floor, developed over a 2.2-m distance before encountering the plume source. The flow depth in the test section was approximately 0.25 m, the turbulence levels in the free stream [defined as root mean square (rms) turbulent velocity divided by free stream velocity] were approximately 2%, and the test section (3 m long by 0.6 m wide) was free from secondary flows.
33. Fluorescent dye, rhodamine 6G, was used as an analog of a dissolved odorant. A solution of the dye of 20 parts per million was pumped at 0.05 ml/s from an "odor source" designed to mimic a diffusive-type release of a scalar from a flush bed-level source. This source was a hole (1 cm in diameter) in the flume floor filled with porous foam to provide a uniform flow across the source exit, as described (*5*). The dye was visualized using a planar laser–induced fluorescence technique, as described (*5*). The apparatus consisted of a Coherent Innova 90 argon-ion laser and optics for focusing and scanning the laser beam across the image area. We used vertical laser scans, positioned parallel to the flow on the centerline of the flume. The focused laser beam (0.28 mm in width) was scanned across the image area (thus creating a light "sheet") with a moving-magnet optical scanner. The laser sheet entered the water through a thin glass plate on the free surface of the water and was reflected up from the bottom of the flume by a mirror. Because rhodamine 6G has a central emission (fluorescence) wavelength of 555 nm, a 540-

to 570-nm notch filter was used on the video camera (described below) to eliminate wavelengths other than the fluoresced light. We used the calibration technique, as described (*5*), to relate the brightness of the pixels on the video images to actual dye concentration.

34. Videos of the antennules were made (framing rate, 250 Hz; shutter speed, 0.004 s) through a 55-mm macro lens (field image, 3.62 cm by 3.16 cm) in a high-speed video system. Videos were analyzed with NIH Image 1.62 software. In each frame, a transect was run through the aesthetasc array parallel to the lateral filament of the antennule; the brightness of each pixel was measured and converted to dye concentration. A transect of the same length, shape, and orientation was made for a virtual antennule at a position 2.6 mm below the tips of the guard hairs, where the dye was not affected by the antennule. Because the structures in the dye plume were advected downstream at 7 cm/s at the height of the antennule within the benthic boundary layer, the transect for a virtual flick was made 1.4 mm upstream and five frames earlier than the transect for the real antennule with which it was compared.
35. An *F* test for equality of variance was done to compare the temporal variance of concentrations encountered by the midpoint of the real versus the virtual antennule for each flick, each return, and each pause ($P < 0.05$, $n = 11$ frames). During the leaky flick downstrokes, there was no difference between the variance of real and virtual antennules in 48% of the flicks, the variance of real was greater than that of virtual antennules in 27% of flicks, and the variance of virtual was greater than that of real antennules in 25% of flicks. In contrast, during the nonleaky return strokes and pauses, when the aesthetasc array held the water sample that had penetrated the array during the flick, the variance of the virtual antennule was greater than that of the real antennule in 96 and 98% of the cases, respectively, which were significantly more than expected under the hypothesis of independence (chi square test, post hoc cell contributions, $P < 0.05$). Similar patterns were shown by all antennules tested ($n = 3$).
36. Péclet number (Pé) characterizes the importance of fluid motion (advection) relative to molecular diffusion in a mass transport process. For hairs in an array, Pé $= LU/D$, where L is hair diameter, U is peak water velocity midway between adjacent hairs, and D is the diffusion coefficient. When Pé is $\sim$1, advection and molecular diffusion are equally important; when Pé is large, advection dominates. For *P. argus*, Pé's during a flick downstroke and upstroke are 1300 and 100, respectively (*25*); thus, advection is much more important than diffusion in transporting odorants or dye in the aesthetasc array. During the pause, when ambient currents do not penetrate the aesthetasc array of an antennule pointing upstream (Fig. 1), Pé is close to zero, and molecular diffusion is the dominant transport mechanism. The rms displacement of molecules by diffusion during a pause of 0.4 s is 33 μm; hence, the spatial distribution of dye filaments within the hair array is altered little, yet there is ample time for molecules in the water trapped between hairs to diffuse to the aesthetasc surfaces (*25*). A model of advection and diffusion of odor filaments through the aesthetasc arrays of flicking stomatopod antennules also showed little diffusive spread of odor filaments on such a time scale (*23*).
37. An *F* test for equality of variance was done to compare the spatial variance of concentrations encountered along the real antennule versus that along the virtual antennule for each flick, each return, and each pause ($P < 0.05$, $n = 210$ positions). During the leaky flick downstrokes, the variance along the real antennule was significantly less than that along the virtual for 59% of the flicks, was greater in 31%, and was the same in 10%. In contrast, during the nonleaky return strokes and pauses (when the aesthetasc array held the water sample that had been blurred during the flick), the variance along the virtual antennule was greater than that along the real in 83 and 81% of the cases, respectively, which were significantly more than expected under the hypothesis of independence (chi square test, post hoc cell contributions, $P < 0.05$), whereas virtual was less than real in 6 and 8% of the cases, respectively, which were significantly fewer than expected. Similar patterns were shown by all antennules tested ($n = 3$).
38. G. Gomez, J. Atema, *J. Exp. Biol.* **199**, 1771 (1996).
39. C. A. O'Riordan, S. G. Monismith, J. R. Koseff, *Limnol. Oceanogr.* **38**, 1712 (1993).
40. Supported by Office of Naval Research grants N00014-96-1-0594, N00014-97-1-0706, and N00014-98-1-0775. We thank G. Wang for technical assistance.

22 June 2001; accepted 24 October 2001